# Synthesis and Ionic Conductivity of Polymer Electrolytes Based on a Polyphosphazene with Short Side Groups

J. Paulsdorf,[†] N. Kaskhedikar,[†,‡] M. Burjanadze,[†] S. Obeidi,[§] N. A. Stolwijk,[§] D. Wilmer,[|] and H.-D. Wiemhöfer*[,†]

*Institute for Inorganic and Analytical Chemistry, Corrensstrasse 30, International NRW Graduate School of Chemistry (GSC−MS), Corrensstrasse 30, Institute for Material Physics, Wilhelm-Klemm-Strasse 10, and Institute for Physical Chemistry, Corrensstrasse 30, University of Münster and SFB 458, 48149 Münster, Germany*

*Received July 16, 2005. Revised Manuscript Received January 4, 2006*

Random copolymers of the polyphosphazene $[NPR_2]_n$ have been synthesized via living ionic polymerization with mixed substituents at the phosphorus atoms (i.e., R = bis(2-methoxy-ethyl)amino and *n*-propylamino). The polymers melt at 190 °C and start to decompose above 300 °C. Thin polymer electrolyte membranes were prepared by solution casting with dissolved lithium triflate ($LiSO_3CF_3$) and with NaI. The transparent membranes showed favorable mechanical properties below 100 °C. $T_g$ values ranged between −50 and −36 °C. Membranes with 10 wt % $LiSO_3CF_3$ (corresponding to the atomic ratio Li/(O + N) = 1/30) showed rather low conductivities between $3.2 \times 10^{-7}$ S cm$^{-1}$ at 30 °C and $1.9 \times 10^{-5}$ S cm$^{-1}$ at 100 °C as determined from impedance measurements. The dispersion of 4 wt % $Al_2O_3$ nanoparticles in the polyphosphazene membranes with 10 wt % $LiSO_3CF_3$, however, leads to an increase of the conductivities by 2 orders of magnitude, that is, $1.0 \times 10^{-5}$ S cm$^{-1}$ at 30 °C and $1.5 \times 10^{-3}$ S cm$^{-1}$ at 100 °C. The heterogeneously doped salt-in-polymer membranes thus combine good mechanical stability with a high ionic conductivity. The temperature dependence of the conductivity data was analyzed in terms of the MIGRATION model, which gives a consistent explanation of the non-Arrhenius dependence.

## Introduction

Since the first investigations on ion conduction in PEO (=poly(ethylene oxide)) salt systems by Fenton et al., many efforts have been made to prepare polymer electrolytes with enhanced conductivity.[1] Although the etheric oxygen of the polymer chains provides a good solvation of lithium ions, crystalline domains in the PEO-based polymer electrolytes present at temperatures below 60 °C permit only low conductivities, for example, $10^{-7}$ S cm$^{-1}$ for a $LiClO_4$–PEO system with Li/O = 1/8 at ambient temperature.[2]

Inorganic polymers with silicon or phosphorus in the main chain, for example, polysiloxanes $[OSiR_2]_n$ and polyphosphazenes $[NPR_2]_n$, show an increased chain mobility together with low $T_g$ values and accordingly a higher tendency to form amorphous regions.[3] All of these factors are considered to improve the mobility of dissolved ions. Combining these properties with suitable side groups that favor ion solvation is a suitable approach toward polymer electrolytes with improved conductivities as was first shown by Blonsky et al.[4,5] They applied a polyphosphazene with short oligoether side chains, that is, poly[bis(methoxyethoxyethoxy)-phosphazene] (=MEEP), as a polymer electrolyte matrix and observed room-temperature conductivities as high as $10^{-5}$ S cm$^{-1}$, as well as a very low glass transition temperature of −84 °C.[4,5] Unfortunately, the latter also leads to relatively poor dimensional stability of the almost gellike MEEP and requires an additional cross linking.

Apart from MEEP, polyphosphazenes with other substituents were tested as polymer electrolytes. Allcock et al. carried out systematic investigations on a large number of polyphosphazenes with linear and branched etheric side chains as well as mixed substituents.[6] Chen-Yang et al. measured ionic conductivities of various lithium and silver salt−polymer electrolytes based on polyphosphazenes substituted with linear primary amines and alkoxides.[7−10] They also examined the solvating properties of the oxygen and nitrogen atoms in the side chains and the main chain of the salt−polymer systems.

* To whom correspondence should be addressed. Fax: +49 251 83 33193. E-mail: hdw@uni-muenster.de.
[†] Institute for Inorganic and Analytical Chemistry.
[‡] International NRW Graduate School of Chemistry (GSC−MS).
[§] Institute for Material Physics.
[|] Institute for Physical Chemistry.

(1) Fenton, D. E.; Parker, J. M.; Wright, P. V. *Polymer* **1973**, *14*, 589.
(2) Fertoni, P. G.; Chiodelli, G.; Magistris, A.; Sanesi, M. *Solid State Ionics* **1986**, *18−19*, 265.
(3) Mark, J. E.; Allcock, H. R.; West, R. *Inorganic Polymers*; Prentice Hall: Englewood Cliffs, NJ, 1992.
(4) Blonsky, P. M.; Shriver, D. F.; Austin, P.; Allcock, H. R. *J. Am. Chem. Soc.* **1984**, *106*, 6854.
(5) Blonsky, P. M.; Shriver, D. F.; Austin, P.; Allcock, H. R. *Solid State Ionics* **1986**, *18−19*, 258.
(6) Allcock, H. R. *Chemistry and Applications of Polyphosphazenes*; Wiley & Sons: Hoboken, NJ, 2003.
(7) Chen-Yang, Y. W.; Hwang, J. J.; Kau, J. Y. *J. Polym. Sci., Part A: Polym. Chem.* **1997**, *35*, 1023.
(8) Chen-Yang, Y. W.; Hwang, J. J.; Chang, F. H. *Macromolecules* **1997**, *30*, 3825.
(9) Chen-Yang, Y. W.; Hwang, J. J.; Huang, A. Y. *Macromolecules* **2000**, *33*, 1237.
(10) Chen-Yang, Y. W.; Chen, H. C.; Lin, F. J.; Liao, C. W. *Solid State Ionics* **2003**, *3*, 383.

10.1021/cm051556u CCC: $33.50 
Published on Web 02/02/2006

**Scheme 1. Reagents and Steps in the Synthesis of BMEAP**

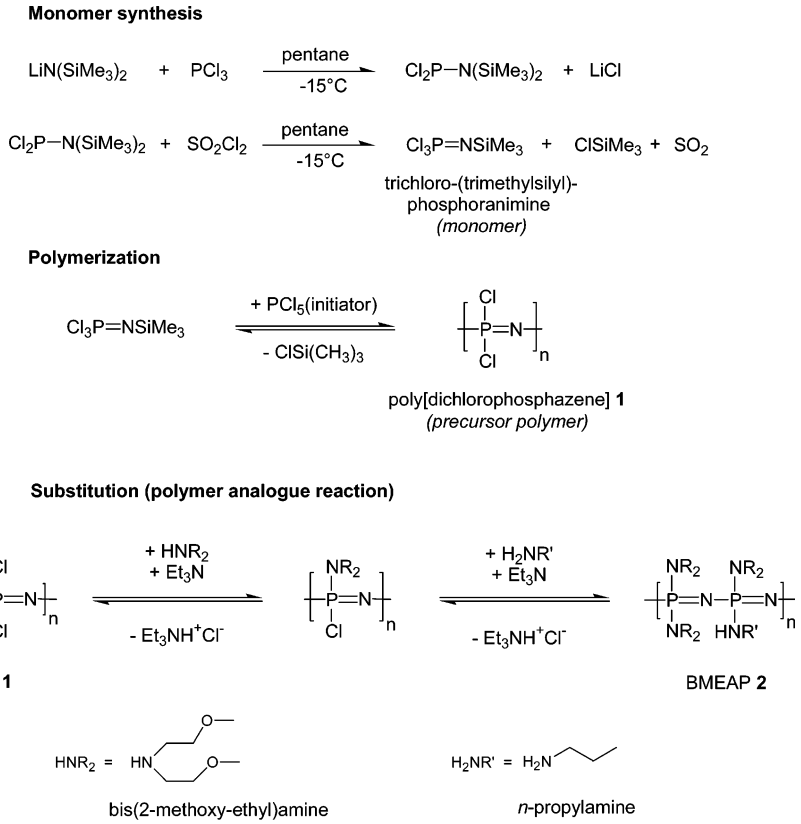


Considerable efforts have been made in the past years to investigate the potential of varying the substituents of the polyphosphazenes to modify and optimize the chemical and physical properties for different applications.[6] There has been also large progress concerning the availability of synthetic routes to high-quality polyphosphazenes. Most often, the chlorine-substituted $(NPCl_2)_n$ **1** is taken as a central precursor polymer. A huge number of different polyphosphazene derivatives can be produced by polymer analogue substitution of the chlorine atoms with a wide variety of nucleophiles such as alkoxides or amines. For the synthesis of the precursor polymer, the living cationic polymerization of the monomer trichloro(trimethylsilyl)phosphoranimine, $Cl_3P{=}NSiMe_3$, at ambient temperature with $PCl_5$ as initiator[11−13] proved to be a very favorable route toward well-defined linear polymers with nearly 100% yield and low polydispersity. It represents a good alternative to the classic thermal, ring-opening polymerization of cyclic hexachlorophosphazene, $(NPCl_2)_3$.[3] The recently reported high-yield synthesis of the monomer $Cl_3P{=}NSiMe_3$ by Manners et al.[14] now makes the living polymerization route most attractive.[15]

In this contribution, we have synthesized and investigated a polyphosphazene system substituted mainly with bis(2-methoxy-ethyl)amine, a branched secondary amine. The polymer will be referred to in the following by the acronym BMEAP. The motivation for this choice was to achieve good mechanical properties of the resulting polymer. The side chains in BMEAP are shorter than those in the classic MEEP, admitting a higher influence of the polymer backbone on the solvation properties and molecular mobility. The solvating effect on salts is supported by the oxygen and nitrogen atoms of the side chains and presumably also by the nitrogen atoms of the polyphosphazene backbone. The branched short side chains should lead to a better dimensional stability as compared to a linear etheric substituent. Because full substitution by a secondary amine is known to be difficult, a primary amine (*n*-propylamine) has been added subsequently to remove remaining chlorine in the polymers, which otherwise may be a source of instability.

## Experimental Section

**Polymer Synthesis.** Our preparation of the precursor polymer poly[dichlorophosphazene] **1** was described in detail in a previous publication.[15] The only modifications here were to lower the reaction temperature to −15 °C by an ice−salt mixture and to use a slight excess of $PCl_3$ in the monomer synthesis of Scheme 1. The latter helped to prevent the formation of $ClN(SiMe_3)_2$, which is known to be a strong polymerization inhibitor. All other steps are described in the following. Scheme 1 illustrates the basic reaction sequence.

Tetrahydrofuran (THF, 99.9%, Riedel-de Haën), pentane (98%, Baker), and toluene (99.7%, Scharlau) were distilled from sodium benzophenone ketyl. Phosphor trichloride ($PCl_3$, 99%, Merck) and sulfuryl chloride ($SO_2Cl_2$, 98%, Merck) were freshly distilled before use. Bis(2-methoxy-ethyl)amine (BMEA, Aldrich, 99%), triethylamine ($Et_3N$, 99%, Merck), and *n*-propylamine (Merck, >99%) were dried over molecular sieves (4 Å) prior to use. Lithium triflate

(11) Allcock, H. R.; Nelson, J. M.; Reeves, S. D.; Honeyman, C. H.; Manners, I. *Macromolecules* **1997**, *30*, 50.
(12) Allcock, H. R.; Nelson, J. M.; Reeves, S. D.; Crane, C. A.; Manners, I. *Macromolecules* **1997**, *30*, 2213.
(13) Allcock, H. R.; Reeves, S. D.; de Denus, C. R.; Crane, C. A. *Macromolecules* **2001**, *34*, 748.
(14) Wang, B.; Rivard, E.; Manners, I. *Inorg. Chem.* **2002**, *41*, 783.
(15) Paulsdorf, J.; Burjanadze, M.; Hagelschur, K.; Wiemhöfer, H.-D. *Solid State Ionics* **2004**, *169*, 25.

($LiSO_3CF_3$, purum, Fluka) and phosphorus pentachloride ($PCl_5$, sublimed in a vacuum) were stored under nitrogen in a glovebox. Sicapent ($P_2O_5$, Merck), tetrabutylammonium bromide (Merck Schuchardt, p. a.), sodium iodide (NaI, Aldrich, >99.5%), and $Al_2O_3$ nanoparticles (Aldrich, <40 nm) were used as received. All reactions were carried out under strictly dry conditions and using standard Schlenk techniques.

Two series of syntheses have been carried out to examine the effects of different reaction conditions during substitution (room temperature (a) and reflux (b)) and purification (dialysis against THF (c) and water (d)) on the material properties of the resulting BMEAP compounds.

For the first experiments, $(NPCl_2)_n$ **1** (28.39 mmol, 3.29 g, 1 equiv) was dissolved in 50 mL of freshly distilled THF and evenly distributed to two 100 mL round-bottom flasks (a, b). With respect to the amount of chlorine (2 equiv) in **1**, a 2-fold excess of $Et_3N$ (57 mmol, 7.9 mL, 4 equiv) and bis(2-methoxy-ethyl)amine (57 mmol, 8.35 mL, 4 equiv) was added via syringe to each flask. Triethylammonium chloride ($Et_3NH^+Cl^-$) started to precipitate after a few minutes. To acchieve a maximum degree of chlorine substitution despite the moderate reactivity of the secondary amine, the reaction was allowed to proceed for 70 h at room temperature (the product is denoted as **2a** in the following). To achieve an even higher degree of substitution by the secondary amine, in a second approach, we also carried out the substitution under reflux in boiling THF for 70 h (the polymer products obtained under these conditions are denoted as **2b**). In both cases, some chlorine remained in the polymer, and, therefore, *n*-propylamine (57 mmol, 4.7 mL, 4 equiv) as a more reactive nucleophile was allowed to react with **2a** and **2b** for another 48 h at room temperature. This finally led to a complete removal of the rest of the chlorine. Afterward, the precipitated $Et_3NH^+Cl^-$ was separated by centrifugation, and THF was removed under vacuum.

The clear and viscous solutions were dialyzed for 6 days against distilled water, using membranes of regenerated cellulose (RC) with a molecular weight cutoff (MWCO) of 12.000−14.000 D. In this step, traces of salt, reagents from the syntheses, and short-chained species were removed. After having been precipitated two times from THF solution in water, the purified polymeric products were dried in an oven at 60 °C for 3 days to give light yellow waxlike poly[(bis(2-methoxy-ethyl)amino)$_x$(propylamino)$_{2-x}$phosphazene], abbreviated in the following as BMEAP **2a** (35.2% yield) and BMEAP **2b** (28.7% yield).

The second experiment has been carried out at room temperature, similar to (a) but at even longer reaction times. $(NPCl_2)_n$ **1** (44.9 mmol, 5.16 g, 1 equiv) was dissolved in 150 mL of THF, and a 2-fold excess of $Et_3N$ (180 mmol, 23.9 mL, 4 equiv) and bis(2-methoxy-ethyl)amine (180 mmol, 26.3 mL, 4 equiv) was added via syringe. The reaction was allowed to proceed at room temperature for 96 h. Subsequently, the second substitutent (*n*-propylamine;180 mmol, 14.8 mL, 4 equiv) was added, and the reaction proceeded for another 96 h. Removal of the precipitated $Et_3NH^+Cl^-$ by centrifugation and of the THF under vacuum led to a clear and viscous solution.

This time, the final purification was done in two different ways: one series of samples was dialyzed against THF for 5 days (RC with MWCO 12.000−14.000 D) and dried in an oven at 60 °C for 3 days to give poly[(bis(2-methoxy-ethyl)amino)$_x$(propylamino)$_{2-x}$-phosphazene], BMEAP **2c** (31% yield). Another series of samples, specified as BMEAP **2d** in the following, was dialyzed against distilled water instead of THF. The yield was 53% in this case.

BMEAP **2e** was synthesized and characterized similarly to **2a**. It was applied as host polymer for experiments on polymer electrolyte membranes doped with $Al_2O_3$ nanoparticles.

**Table 1. Ratio of the Two Substituents As Estimated from $^1$H NMR**

| | BMEAP sample | | | | |
|---|---|---|---|---|---|
| | **2a** | **2b** | **2c** | **2d** | **2e** |
| bis(2-methoxy-ethyl)amino | 60% | 55% | 58% | 47% | 60% |
| *n*-propylamino | 40% | 45% | 42% | 53% | 40% |

**NMR.** NMR was used to verify the intended substitution in samples **2a**−**2e** and to determine the molar ratio of the two different substituents in each case. Table 1 shows the results. The $^1$H, $^{13}$C, and C,H-COSY NMR spectra were measured with a Varian 400 plus spectrometer, and $^{31}$P NMR spectra were measured with a Bruker ARX 300. The polymer samples **2a**−**2e** were dissolved in $CDCl_3$ and referenced internally to TMS (tetramethylsilane) ($^1$H, $^{13}$C, and C,H-COSY), and externally to 85% $H_3PO_4$ for $^{31}$P NMR. The carbon peaks could be identified easily, but in the proton spectrum some peaks were overlapping. With an additional two-dimensional $^{13}$C−$^1$H-shift correlated spectroscopy measurement (C,H-COSY), the assignment of the proton peaks could be verified unambiguously. In the $^{31}$P spectra, the phosphorus of the base chain gives a broad signal extending from −5 to 5 ppm having a maximum at 2.7 ± 0.6 ppm with two small shoulders in the range between +1 and −5 to 2 ppm. The three resonances are to be expected for a random substitution by the two applied substituents, which produce three different substitution patterns of phosphorus. Because of the strong overlap between the three signals, a peak area analysis could not be done by $^{31}$P NMR.

A small additional peak in the $^{31}$P NMR at 17 ppm is assigned to the corresponding fully substituted cyclotriphosphazene. The cyclic phosphazene is a typical product of chain degradation and is another hint to the partial chain cleavage during the substitution reaction. Detailed NMR data are given in the Supporting Information. The NMR spectra of all BMEAP products **2a**−**2e** gave no evidence for impurities such as $Et_3NH^+Cl^-$ or reagents from the synthesis step.

***M*$_w$ Distribution from GPC.** We dissolved the polymer samples **2a**−**2d** in THF and determined the molecular weight distribution ($M_w$) and the polydispersity ($d$) by gel permeation chromatography (GPC). 0.1 wt % tetrabutylammonium bromide was dissolved in the eluent (THF). The Agilent 1100 series isocratic pump and RI-detector ($\eta$-1001 viscosimeter from WGE Dr. Bures) were equipped with two PSS-SDV linear XL columns (8 × 300 mm, 5$\mu$) from Polymer Standards Service (PSS, Mainz) and calibrated with polystyrene standards (ReadyCal, PSS, Mainz).

The precursor polymer $[NPCl_2]_n$ resulting from our synthesis usually shows polydispersities in the range 1.4−1.8 and an average molecular weight around $1.6 \times 10^5$ D (number average). Compared to this, all product polymers after substitution showed a clear broadening of the molecular weight distribution as can be seen in Table 2. Furthermore, the polymers **2a**, **2b**, and **2c** showed additional shoulders in the GPC elution curves. The comparison between the precursor polymer and the BMEAP samples gives evidence for chain cleavage during the substitution reaction. The substitution at elevated temperatures even enhances this effect as can be seen in going from **2a** (reaction at room temperature) to **2b** (boiling THF). An increase of the reaction time for the nucleophilic substitution at room temperature tended to enhance the broadening of the molecular weight distribution. Our experience is that substitution by amines and in particular by secondary amines tends to enhance gradually causes chain cleavage of the polyphosphazenes much more than substitution by alkoxide ions. For alkoxy-substituted polymers, we usually found polydispersities in the range of 1.5−1.8.

The GPC spectra also revealed differences between the two polymer materials **2c** and **2d** after substitution, although they have

**Table 2. Average Molecular Weights ($M_w$) and Polydispersities ($d$) of the Precursor Polymer $[NPCl_2]_n$ (=1) and the BMEAP Samples Determined by GPC[a]**

| sample | average $M_w$ [D] (additional maxima in brackets) | average number of monomer units | polydispersity |
|---|---|---|---|
| **1** | $1.6(\pm 0.2) \times 10^5$ (no shoulder) | $1370 \pm 170$ | 1.5 |
| **2a** | $5.0 \times 10^4$ ($5.9 \times 10^3$; $5.4 \times 10^4$) | 205 | 3.8 |
| **2b** | $4.6 \times 10^4$ ($4.2 \times 10^3$; $6.4 \times 10^4$) | 185 | 4.8 |
| **2c** | $2.7 \times 10^4$ (weak shoulder at $8 \times 10^4$) | 110 | 2.8 |
| **2d** | $3.0 \times 10^5$ (no shoulder) | 1300 | 3.8 |
| **2e** | $1.4 \times 10^5$ (no shoulder) | 600 | 4.2 |

[a] For **2a**, **2b**, and **2c**, the MW distributions showed additional shoulders of which the corresponding peak maxima are given in brackets.

been synthesized following identical procedures. A tentative explanation is that the dialysis against THF as applied for **2c** might have led to enhanced loss of polymer fractions as compared to dialysis of **2d** against water. Nevertheless, the BMEAP samples **2c**, **2d**, and **2e** were the best with respect to homogeneity and polydispersities. Therefore, they were applied as host polymers for the preparation of polymer electrolyte membranes.

**Membrane Preparation.** Polymer electrolyte membranes were obtained by casting THF solutions of polymer and salt into circular Teflon moulds with 4 cm interior diameter and 2 cm height. BMEAP **2c** and suitable amounts of lithium triflate (=$LiSO_3CF_3$), 2, 5, and 10 wt %, were both dissolved in THF. After the resulting viscous solutions were poured into the Teflon moulds, the solvent was allowed to evaporate very slowly at room temperature so that homogeneous and free-standing films of ~120 $\mu$m thickness formed after 3 days. The elastic and nonbrittle membranes could easily be removed from the moulds. They were dried in an oven (60 °C) and stored in a desiccator over Sicapent. After drying, the polymer membranes still were elastic.

For the impedance measurements, they could be cut easily in the form of circular disks and placed between planar stainless steel electrodes. Because of the added salt, the samples were slightly hygroscopic and had to be stored in a glovebox and measured in a constant flow of dry nitrogen (100 mL/min).

To prepare sodium iodide containing BMEAP membranes, NaI (10 wt % in polymer **2d**) was dissolved in dry ethanol, mixed with the solution of the polymer **2d** in THF, and cast into a Teflon mould, followed by the same drying steps as for the $LiSO_3CF_3$-doped membranes.

Membranes with dispersed $Al_2O_3$ nanoparticles were prepared as follows. BMEAP **2e** was dissolved together with 10 wt % lithium triflate in THF. Various amounts (2, 4, 6, 8, and 10 wt %) of $Al_2O_3$ nanoparticles (<40 nm) were added and dispersed in the solution by rigorous stirring and subsequent exposure to an ultrasonic bath (15 min). The further preparation of the polymer membranes was carried out in the same way as described above. Flexible, elastic composite polymer electrolyte membranes were obtained after drying.

**FT-IR.** All polymers **2a**−**2d** and also the polymer electrolytes prepared from **2c** and **2d** were cooled with liquid nitrogen and ground to powder that could be pressed between KBr windows and measured in a Bruker IFS 113v IR spectrometer.

**Differential Scanning Calorimetry (DSC).** DSC was applied to determine glass transition temperatures ($T_g$) and melting transitions (mt) in our polymer electrolyte materials. We used a Netzsch DSC 204 at a heating rate of 10 K/min between −160 and 180 °C. Heating up and cooling to the initial temperature was repeated three times to study thermal hysteresis.

**Impedance Measurements.** The polyelectrolyte membranes were cut into disks of 11.28 mm diameter (→ A = 1 cm$^2$) and sandwiched between two ion blocking stainless steel foils during the measurement. The distance between the electrodes could be adjusted by a micrometer screw to ensure that the samples were contacted properly. In addition, a steel spring applied a constant mechanical pressure to the sample. The measurements were carried out in a closed vessel under an atmosphere of dry nitrogen. The temperature of the vessel was controlled externally via thermostats: Thermo Haake Kryostat (−10 to 25 °C, ethanol) and Thermo Haake Phönix P2 (25−150 °C, silicon oil). The impedance measurements were carried out using an Agilent 4192A impedance spectrometer with a frequency range of 5 Hz to 13 MHz.

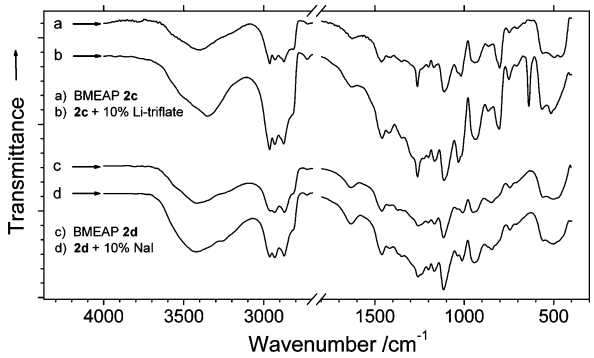


**Figure 1.** Characteristic IR absorptions of BMEAP, as compared to the corresponding lithium and sodium salt mixtures: (a) BMEAP **2c**, (b) BMEAP **2c** + 10% $LiSO_3CF_3$, (c) BMEAP **2d**, (d) BMEAP **2d** + 10% NaI.

## Results and Discussion

**FT-IR Results.** We first discuss the results of FT-IR and DSC measurements before discussing the ionic conductivities. In Figure 1, the spectra of the pure polymers BMEAP **2c** and **2d** are compared to the corresponding polymer electrolyte membranes after dissolving 10 wt % $LiSO_3CF_3$. The broad band around 3400 cm$^{-1}$ in all spectra is assigned to moisture in KBr. The characteristic absorption spectra for **2c** and **2d** are very similar. The following discussion is based on a comparison with published data for related compounds.[10,16,17]

For the polymer **2c** with dissolved $LiSO_3CF_3$, the intensity of the $SO_2$ deformation band at 638 cm$^{-1}$ grows with increasing salt concentration and shifts to slightly higher frequencies as expected. This is most likely due to the interaction of the $LiSO_3CF_3$ with the ether oxygen of the side groups and the formation of a "$CF_3SO_3^-$:$Li^+$:$OR_2$" complex as was also found for related polyphosphazenes.[17] With increasing salt concentration, the absorption of the anionic $SO_3^-$ (at about 1032 cm$^{-1}$) starts overlapping the

(16) Colthup, N.; Daly, L.; Wiberley, S. *Introduction to Infrared and Raman Spectroscopy*, 2nd ed.; Academic Press: New York, 1975.
(17) Luther, T. A.; Stewart, F. F.; Budzien, J. L.; LaViolette, R. A.; Bauer, W. F.; Harrup, M. K.; Allen, C. W.; Elayan, A. *J. Phys. Chem. B* **2003**, *107*, 3168.

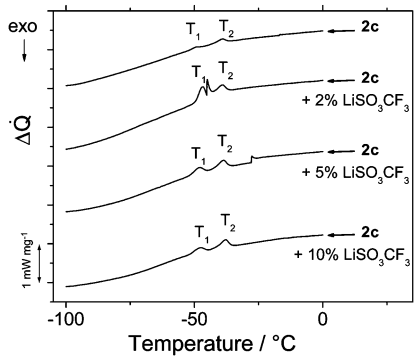


**Figure 2.** DSC results of BMEAP **2c** and the corresponding polymer−$LiSO_3CF_3$ mixtures between −100 and 0 °C.

C−N resonances of the primary amino group at 1018 $cm^{-1}$. The intensities of the P−N−C stretching modes of the side groups at 750 and 863 $cm^{-1}$ increase with increasing $LiSO_3CF_3$ concentration, reaching a maximum at 5 wt % $LiSO_3CF_3$, and then significantly decrease to a minimum for the sample with 10 wt % $LiSO_3CF_3$, as compared to pure **2c**. This gives evidence for the interaction of the cations (or cation complexes) with the amino group of the side chain.

For 10 wt % $LiSO_3CF_3$, the $OCH_3$ valence bond absorption (at 2820 $cm^{-1}$) slightly weakens, and the intensities of the C−O−C stretching at 1113 $cm^{-1}$ decrease constantly by almost 30% to a minimum. This bond weakening might be due to the interaction between lithium cations and the free electron pairs of the ether oxygen.

For the polymer **2d** with dissolved sodium iodide, the expected additional bands due to NaI in the range of 3560−3415 $cm^{-1}$ and in the fingerprint region at 1620, 613, and 471 $cm^{-1}$ are hidden by absorption bands of the polymer. The intensity of the C−O−C stretching band at 1116 $cm^{-1}$ decreases by 25%, very similar to the **2c**−$LiSO_3CF_3$ system. The P−N−C stretching modes slightly increase in intensity comparable to the samples with 2.5 and 5 wt % $LiSO_3CF_3$.

The incorporation of $Al_2O_3$ has apparently no effect on the position of the C−O−C stretching bands at 1116 $cm^{-1}$, but the $OCH_3$ valence bonds slightly shifted to a minimum of 2824 $cm^{-1}$ for the sample with 4% $Al_2O_3$, which also showed the highest conductivity. This shift might be due to interactions between OH-groups (Lewis acid) present on the surface of the alumina particles and terminal ether-functions (Lewis base) of the polymer side chains.[10] In addition, the wavenumber of the C−N stretching mode is minimal for the same composite polymer electrolyte (1164 $cm^{-1}$), which can result from an apparently higher amount of $Li^+$ displaced from the etheric to the amino moieties by the alumina particles occupying the outer regions of the polymeric host.

Overall, the spectra give evidence for the interaction of the salt with both the oxygen and the nitrogen atoms of the side chains, but the main chain nitrogen remains unaffected.[18] There is also a correlation between the increase of the ionic conductivity and the increasing interaction of ions with the side groups of the polymer.

**DSC Results.** Typical DSC results are illustrated in Figures 2 and 3. For BMEAP **2a** and **2b**, we found a glass transition with an onset around −49 °C, superimposed by two first-order transitions ($T_1$, $T_2$) at −44 and −36 °C and a third one ($T_3$) around 23 °C, slightly shifted toward lower temperatures for **2b** (see Table 3). The presence of two transitions suggests the existence of a microphase heterogeneity within the polymer, which is enhanced by the presence of dissolved salt. Heating up to 350 °C showed a fourth transition due to melting at 179 °C, followed by irreversible decomposition. This corresponds reasonably well to the independently determined bulk melting temperatures (see Table 3). Below this melting point, the materials appeared as waxlike amorphous solids.

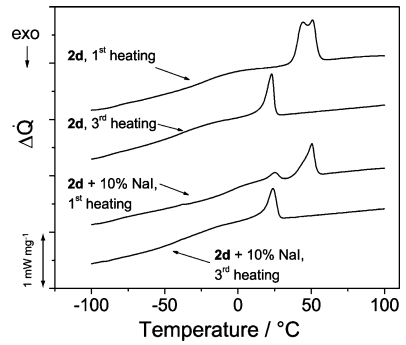


**Figure 3.** DSC results of BMEAP **2d** and corresponding results for the 10 wt % NaI sample; the first and third runs are shown for both samples.

**Table 3. Temperatures for Thermal Transitions Observed during DSC of the Pure Polymers 2a−2d and Corresponding Salt-in-Polymer Systems**

| BMEAP sample | $T_1$/°C | $T_2$/°C | $T_3$/°C | $T_{mp}$/°C[a] |
|---|---|---|---|---|
| **2a** | −44.2 | −36.2 | 23.1 | 165−190 |
| **2b** | −44.7 | −36.2 | 25.4 | 150−170 |
| **2c** | −50 ($T_g$) | −38.6 | | 140−147 |
| **2c** + 2% $LiSO_3CF_3$ | −49.4 | −41.8 | | |
| **2c** + 5% $LiSO_3CF_3$ | −51.5 | −42.8 | | |
| **2c** + 10% $LiSO_3CF_3$ | −51.5 | −42.2 | | |
| **2d** | | −40 ($T_g$) | 22.9 | 148−162 |
| **2d** + 10% NaI | | −40 ($T_g$) | 23.9 | |
| **2e** | | −40 ($T_g$) | | 150−160 |
| **2e** + 10% $LiSO_3CF_3$ | −45 | −40 | | not meas. |
| +2% $Al_2O_3$ | | −40.4 | 30.9 | not meas. |
| +4% $Al_2O_3$ | | −41.2 | | not meas. |
| +6% $Al_2O_3$ | | −40.2 | 24.0 | not meas. |
| +8% $Al_2O_3$ | −49.2 | −40.3 | | not meas. |
| +10% $Al_2O_3$ | −50.6 | −37.2 | | not meas. |

[a] The temperature ranges for the bulk melting ($T_{mp}$) have been estimated visually with a SMP10 Stuart Scientific/Bibby Sterilin Ltd., UK, device at heating rates of 20 K/min (coarse) and 2 K/min (fine).

The pure polymer **2c** had a glass transition ($T_g$) starting at −50 °C and a melting transition $T_2$ at −38.6 °C. When $LiSO_3CF_3$ was added, the thermal behavior of all samples changed in nearly the same way: With dissolved salt, no clear $T_g$ could be observed, but melting transitions were seen at about −46 °C and between −40 and −38.6 °C, replacing or hiding a possible glass transition. With higher salt content, the second melting transition $T_2$ shifted slightly to higher temperatures (see Table 3).

BMEAP **2d** and **2e**, which had the highest $M_w$ values of all prepared samples (cf., Table 2), both showed a broad glass transition region with an onset at about −40 °C. Only BMEAP **2d** gave an additional melting between 40 and 50 °C, which shifted to 19 °C after three heating−cooling cycles (see Figure 3). This indicates a higher ordering tendency of the high $M_w$ material.

(18) York, S.; Kellam, E. C., III; Allcock, H. R.; Frech, R. *Electrochim. Acta* **2001**, *46*, 1553.

Polymer **2d** with dissolved sodium iodide showed two first-order transitions at 23 and near −50 °C. As shown in Figure 3, the curve simplified after the third heating cycle and resembled that of pure **2d** below 0 °C. Differences in the DSC curves of **2c** and **2d** may result from a higher content of the secondary amine BMEA in **2c** as compared to **2d**, which probably is also the reason for the tendency to lower bulk melting points of **2c** and **2d** as compared to **2a** and **2b**.

The differences of the various polymer samples in the DSC curves may result from the difference in $M_w$ (cf., Table 2) and in the ratio of the two side groups (cf., Table 1). Yet it is also evident that the polymer tends to form a sort of microphase heterogeneity, which seems to be enhanced after dissolution of salt. One observes a splitting of the glass transition into two nearby thermal transitions (−45 °C/−40 °C) in polymer **2e** after adding the salt. It cannot be excluded that the distribution of salt between the microphases is inhomogeneous.

For the $Al_2O_3$-composite polymer electrolyte based on **2e**, we found melting transitions ($T_2$) around −40 °C (cf., Table 3) with a minimum for 4% and a maximum for 10% $Al_2O_3$, the composite electrolyte samples with the highest and lowest conductivity (cf., Table S-4 in the Supporting Informations). Yet these variations in $T_2$ were not very clearly to evaluate and should be considered as hints rather than as proofs for a correlation between conductivity and thermal behavior. The onset of a weak glass transition point $T_g$ can be found around −50 °C. Again, there is no distinct correlation between addition of $Al_2O_3$ particles and thermal behavior. The samples also revealed a third melting transition around 25 °C ($T_3$), but these were vague and difficult to evaluate from the spectra.

**Impedance Spectra.** For all sample membranes, reproducible values of the temperature-dependent impedance spectra were obtained after two initial heating−cooling runs. This was comparable to the behavior observed in the DSC measurements. Good reproducibility was obtained then in the temperature range of −20 to 100 °C. Above that temperature, the samples tended to flow under the mechanical pressure applied to the electrodes, which changes the membrane thickness. In the following, the results for the two differently doped polymer membranes are discussed.

Polymer electrolyte membranes were prepared from BMEAP **2c** (having 58% substitution by BMEA and 42% by *n*-propylamine at the phosphorus atoms). The $LiSO_3CF_3$ concentrations were 2, 5, and 10 wt %. The corresponding ratios "Li/monomer units" were 1:32, 1:13, and 1:6, respectively. Three N atoms and between two and four O atoms are available per segment for the solvation of cations.

Figure 4 shows the impedance spectra (Bode diagram) for the membrane with 10 wt % $LiSO_3CF_3$. The spectra for other concentrations were comparable. The inset in Figure 4 shows the equivalent circuit that gave a good fit for the observed frequency dependence. In the medium range of frequencies, where the phase angle becomes almost zero, the impedance is represented with good approximation by the ohmic resistance $R_{bulk}$, which was used to calculate the bulk ionic resistivity of the polymer electrolyte membrane.

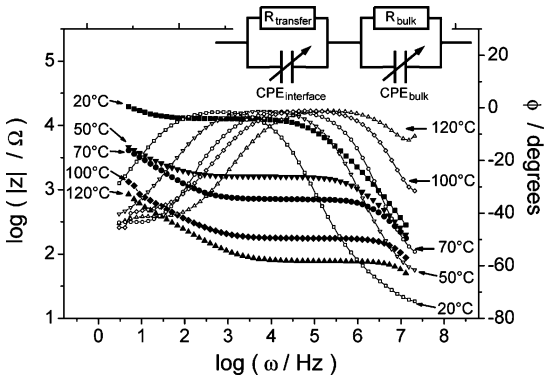


**Figure 4.** Impedance spectra (Bode diagram) for a membrane made from BMEAP **2c** with 10 wt % $LiSO_3CF_3$ and temperatures between 20 and 100 °C: black solid symbols = logarithm of magnitude of the impedance, open symbols = phase angle (membrane thickness, 0.175 mm; surface area, 1.00 $cm^2$). Inset: equivalent circuit used in calculating the conductivities (from $R_{bulk}$).

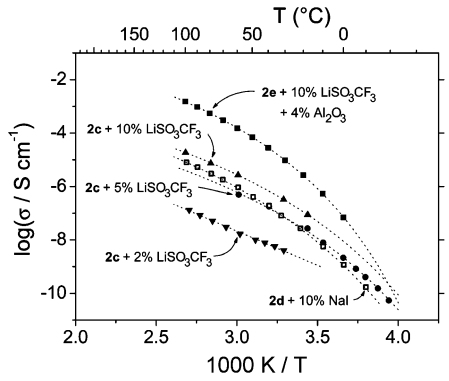


**Figure 5.** Temperature dependence of the conductivities of the polymer electrolyte membranes $LiSO_3CF_3$/BMEAP **2c**, NaI/BMEAP **2d**, and $LiSO_3CF_3/Al_2O_3$/BMEAP **2e**: open symbols = experimental conductivities, dotted lines = fits to the VFT eq 1 and to the CMR eq 2. The fit parameters are listed in Table 4.

The impedance spectra of polymer electrolyte membranes made of BMEAP **2d** mixed with 10 wt % NaI were recorded between −10 and 100 °C. They were similar to those in Figure 4.

**Ionic Conductivities.** Figure 5 shows the temperature-dependent conductivities for the three types of polymer electrolyte membranes $LiSO_3CF_3$/BMEAP **2c**, NaI/BMEAP **2d**, and 10 wt % $LiSO_3CF_3$/4 wt % $Al_2O_3$/BMEAP **2e**. Further results for the ionic conductivities of BMEAP(**2e**)/$Al_2O_3$-composite polymer electrolytes are listed in Table S-3 of the Supporting Information.[19]

Although the molar ratio of NaI to the number of $-NPR_2-$ segments was almost the same as for the 10 wt % $LiSO_3CF_3$-doped polymer, the ionic conductivity with NaI was lower by one-half an order of magnitude and comparable to the **2c** + 5 wt % $LiSO_3CF_3$ sample. The slightly different substitution patterns of polymers **2c** and **2d** (cf., Table 1) cannot explain this finding. The lower ion mobility observed with NaI must be due to less dissociation and/or a reduced solvation by the polymer as compared to $LiSO_3CF_3$. This is in agreement with a recent study by tracer diffusion technique on the related polymer electrolyte NaI + PEO, which gave evidence for a strong contribution of neutral ion pairs and therefore a low amount of mobile ions available for conductivity.[20]

**Table 4. Parameters Derived from a Fit of the Conductivity Data of Figure 5 to the CMR Eq 1[a]**

| parameter | **2c** + 2 wt % $LiSO_3CF_3$ | **2c** + 5 wt % $LiSO_3CF_3$ | **2c** + 10 wt % $LiSO_3CF_3$ | **2d** + 10 wt % NaI | **2e** + 10 wt % $LiSO_3CF_3$ + 4 wt % $Al_2O_3$ |
|---|---|---|---|---|---|
| VFT, eq 1 | | | | | |
| $T_0$/K | 0 | 167 | 173 | 173 | 194 |
| $B$/K | 5953 | 1775 | 1530 | 1790 | 1413 |
| $\sigma_0$/S cm$^{-1}$ | 1.23 | 0.029 | 0.04 | 0.06 | 4.02 |
| CMR, eq 2 | | | | | |
| $a$/S cm$^{-1}$ K | 184 | 410 | 498 | 523 | 2963 |
| $E$*/eV | 0.060 | 0.077 | 0.079 | 0.083 | 0.118 |
| $\sigma$*/S cm$^{-1}$ | 1.0 | 0.989 | 0.998 | 1.005 | 1.00 |

[a] Note that the 2 wt % $LiSO_3CF_3$ sample nearly shows Arrhenius behavior.

Except for the 2 wt % $LiSO_3CF_3$ sample, the temperature dependence of the conductivities showed marked deviations from the Arrhenius law. This is typical for many polymer electrolytes. Many authors used to fit this non-Arrhenius temperature dependence with the empirical Vogel−Fulcher−Tammann (VFT) equation given by

$$\sigma(T) = \sigma_0 \exp\left[\frac{-B}{T - T_0}\right] \quad (1)$$

The parameters $\sigma_0$, $B$, and $T_0$ obtained from such fits for our polymer membranes are given in Table 4. The validity of the VFT relation for the ionic conductivity versus temperature is most often attributed to a strong coupling between ion transport and segmental motions of the polymer. However, there is no straightforward molecular interpretation of the values of the constants $B$ and $T_0$ in the VFT equation, although attempts have been taken to relate the VFT equation to dynamic models for the segmental motion and transport.[21,22]

In the past years, Funke et al. developed a theoretical concept to account for the frequency and temperature dependence of ionic conductivities in disordered and amorphous ionic conducting materials. This MIGRATION concept was shown to yield a very good description of the experimental conductivity as a function of frequency and temperature in a series of fast ion conductors, glasses, and polymer electrolytes.[23,24] Within this model, the authors also derived an equation for supercooled fragile melts, which describes the non-Arrhenius dependence of the ionic conductivity versus temperature as a consequence of the assumptions in the MIGRATION concept. An important advantage of the MIGRATION concept is that the appearing parameters obtained from fitting the temperature dependence are related to high-frequency conductivity of the ions and thus are connected to well interpretable parameters. The high-frequency conductivity can be verified by additional frequency-dependent measurements over a large range of frequencies.[23,24] The non-Arrhenius dependence in the low-frequency limit is a result of the strong dependence of the probability of successful ion jumps from the necessary, but slow lattice reorientation at the new sites.

The rate of successful ion jumps in amorphous polymer electrolytes is limited by the coupling to the molecular relaxation of the interacting polymer. There is a comparable concept in the discussion of dielectric relaxation of polymers.[21] One distinguishes a slow α-relaxation and a faster $\beta$-relaxation, which show different characteristic temperature dependences. In a simplified model, as described in ref 21, the $\beta$-relaxation of a molecule in a polymer is due to a local "rattling" motion in the cage of its neighbors with typical times of the order of $10^{-10}$−$10^{-12}$ s. The $\beta$-relaxation obeys an Arrhenius law with respect to the temperature dependence. The α-relaxation, on the other hand, corresponds to the reorientation of molecules forming a cage and is a slower cooperative process, which obeys a VFT-type temperature dependence. These concepts show considerable analogy to the relaxation processes assumed in the MIGRATION concept with respect to the ion dynamics within an amorphous lattice.

The dc conductivity as a function of temperature $T$ within the MIGRATION concept is written as

$$\sigma_{dc}(T) = \sigma_{hf}(T) \exp\left[-\frac{\sigma^*}{\sigma_{hf}(T)}\right]$$

with

$$\sigma_{hf}(T) = \frac{a}{T} \exp\left[-\frac{E^*}{k_B T}\right] \quad (2)$$

where $\sigma_{hf}(T)$ and $E$* denote the conductivity and the activation energy in the limit of high frequencies. Overall, eq 1 contains the three fit parameters $a$, $E$*, and $\sigma$*. Table 4 shows the corresponding parameter values obtained by fitting the MIGRATION equation to the temperature-dependent conductivities of Figure 5.

Both the VFT equation and the MIGRATION concept yield an excellent fit to the observed conductivities (cf., identical dotted lines in Figure 5). The prefactor $a$ increases proportionally to the salt concentration as expected. This is evidently not the case with the prefactor $\sigma_0$ obtained from the VFT fit (cf., Table 4). The largest increase of $a$ occurs for the sample with nanoparticles, which obviously means that the concentration of mobile species is strongly enhanced there. The (high frequency) activation energy $E$* shows a weak, monotonic increase with the salt concentration, but a

(19) Kaskhedikar, N.; Paulsdorf, J.; Burjanadze, M.; Karatas, Y.; Roling, B.; Wiemhöfer, H.-D. Presented at the Solid State Ionics Conference (SSI-15), Baden-Baden, Germany, July, 2005.
(20) Stolwijk, N. A.; Obeidi, S. *Phys. Rev. Lett.* **2004**, *93*, 125901/1.
(21) Kremer, F., Schönhals, A., Eds. *Broadband Dielectric Spectroscopy*; Springer: Berlin, 2003; p 99.
(22) Gray, F.; Armand, M. In *Handbook of Battery Materials*; Besenhard, J. O., Ed.; Wiley-VCH: Weinheim, 1999; p 499.
(23) Funke, K.; Heimann, B.; Vering, M.; Wilmer, D. *J. Electrochem. Soc.* **2001**, *148*, A395.
(24) Funke, K.; Banhatti, R. D.; Bruckner, S.; Cramer, C.; Krieger, C.; Mandanici, A.; Martiny, C.; Ross, I. *Phys. Chem. Chem. Phys.* **2002**, *4*, 3155.

distinct jump for the sample with dispersed $Al_2O_3$ particles. A reasonable explanation is that the polymer lattice of the homogeneous salt-in-polymer systems is not changing much with the salt concentration and therefore the barriers for the ion jump, too (at high frequencies), but that there is a distinct change of the polymer lattice in the vicinity of dispersed $Al_2O_3$ particles. For all samples, the order of magnitude of $E^*$ is comparable to values found for other materials that were analyzed in terms of the MIGRATION model.[23,24]

The dependence of the conductivity on the $LiSO_3CF_3$ concentration is nonlinear. A large increase is found in going from 2 to 5 wt % $LiSO_3CF_3$. A tentative explanation is that the salt is distributed inhomogeneously (cf., DSC results). This strongly depresses the conductivity at low concentrations, because the salt first concentrates in microphase areas with high salt−polymer interactions leaving a low salt concentration between them. With increasing concentration, the salt starts to be dissolved in larger areas of the polymer membranes, leading to a clear increase of conductivity. Within this hypothesis, the nanoparticle dispersion may enhance the amount of polymer conformations with good salt solubility and good ionic mobility.

The effect of dispersed $Al_2O_3$ nanoparticles (40 nm) is surprisingly strong and thus the most interesting result (cf., Figure 5, further data in Supporting Information). For a concentration of 4 wt % $Al_2O_3$ nanoparticles in BMEAP **2e** + 10 wt % $LiSO_3CF_3$, we found the highest conductivity enhancement with 2 orders of magnitude reaching $1.0 \times 10^{-5}$ S cm$^{-1}$ at 30 °C and still 1 order of magnitude at 90 °C giving $10^{-3}$ S cm$^{-1}$. These conductivities are almost comparable to the values around $3 \times 10^{-5}$ S cm$^{-1}$ at 25 °C reported for polyphosphazenes having oligo ether side chains with two to eight ethoxy groups. A very similar result has already been found recently by Chen-Yang et al.[10] for a polymer electrolyte based on poly[bis(methoxyethoxyethoxy)-phosphazene] with dissolved $LiClO_4$ and 2.5 wt % of dispersed $\alpha$-$Al_2O_3$ particles showing a conductivity enhancement by 1 order of magnitude at room temperature.

Possible factors contributing to this effect are preferred adsorption of cations or anions at the particle surfaces together with space charges that alter the ion concentrations near the particles, or changes of the conformation of the macromolecules (for instance, an unfolding) near the interface due to adsorption. The latter may lead to an increased number of favorable ionic sites and thus to increased ion mobility or increased ion concentration. Chen-Yang et al. explain the conductivity increase by an enhanced salt dissociation and chemisorption of lithium ions on the particle surface.[10] However, using a tracer diffusion technique, Stolwijk et al. recently showed that ion migration in polyether-based salt-in-polymer systems occurs to a large degree by ion pair transport.[20] Therefore, the contribution of internal particle surfaces to the mobility of ion pairs and anions has to be analyzed in more detail in the future.

Sometimes, strongly chemisorbed water at the particles withstanding the drying steps is assumed to contribute to the conductivity enhancement of heterogeneously doped polymers. However, the absorption of water in particle-free membranes from the gas phase resulted in weak or negligible conductivity changes only. It will be a challenge to further investigate the mechanism for the conductivity enhancement by dispersed particles in polymer electrolytes.

## Conclusions

A primary aim was to synthesize modified polyphosphazenes that combine good mechanical properties with good ion conductivities. The mechanical properties of the investigated polymer with small, branched substituents were quite satisfactory, leading to flexible, transparent membranes. The oxygen and nitrogen atoms of the side groups provided good coordination sites for cations and supported a good solubility for the salts.

The ionic conductivity of membranes with dispersed nanoparticles reached conductivity values quite similar to those reported for the classic MEEP.[4,5] A common opinion is that the good ionic conductivity in polyphosphazenes such as MEEP relies on the presence of oligo- or poly(ethylene oxide) side chains with at least three oxygens to provide a good solvation of cations. Our results show that a high ionic mobility is also possible with quite short side groups that are not optimized for strong ion solvation. The strong effect of $Al_2O_3$ nanoparticles shows in addition that heterogeneous doping is a promising route toward further conductivity enhancements.

**Acknowledgment.** We thank Wilma Pröbsting for the DSC measurements and the Deutsche Forschungsgemeinschaft (DFG) for financial support within the Sonderforschungsbereich (SFB) 458.

**Supporting Information Available:** IR absorptions and NMR data tables of **2a**−**2b**, ionic conductivities of BMEAP(**2e**)/$LiSO_3CF_3$/$Al_2O_3$-composite polymer electrolytes (PDF). This material is available free of charge via the Internet at http://pubs.acs.org.

CM051556U